CHINESE OPTICS LETTERS

Vol. 21, No. 9 | September 2023

Adaptive microwave photonic angle-of-arrival estimation based on BiGRU-CNN [Invited]

Yin Li (李 寅)[1], Qiaosong Cai (蔡乔松)[2], Jie Yang (杨 杰)[2], Tong Zhou (周 侗)[3], Yuanxi Peng (彭元喜)[1], and Tian Jiang (江 天)[4*]

[1] Institute for Quantum Information & State Key Laboratory of High Performance Computing, College of Computer Science and Technology, National University of Defense Technology, Changsha 410073, China

[2] National Innovation Institute of Defense Technology, Academy of Military Sciences PLA China, Beijing 100071, China

[3] Beijing Institute for Advanced Study, National University of Defense Technology, Beijing 100000, China

[4] Institute for Quantum Science and Technology, College of Science, National University of Defense Technology, Changsha 410073, China

*Corresponding author: tjiang@nudt.edu.cn

Received March 21, 2023 | Accepted August 29, 2023 | Posted Online September 15, 2023

An adaptive microwave photonic angle-of-arrival (AOA) estimation approach based on a convolutional neural network with a bidirectional gated recurrent unit (BiGRU-CNN) is proposed and demonstrated. Compared with the previously reported AOA estimation methods based on phase-to-power mapping, the proposed method is unnecessary to know the frequency of the signal under test (SUT) in advance. The envelope voltage correlation matrix is obtained from dual-drive Mach–Zehnder modulator (N-DDMZM, $N > 2$) optical interferometer arrays first, and then AOA estimations are performed on different frequency signals with the aid of BiGRU-CNN. A three-DDMZM-based experiment is carried out to assess the estimation performance of microwave signals at three different frequencies, and the mean absolute error is only 0.1545°.

Keywords: microwave photonics; angle-of-arrival; deep learning; adaptive algorithm.
DOI: 10.3788/COL202321.090001

1. Introduction

Angle-of-arrival (AOA) estimation is a vital parameter in passive target perception fields such as radar, wireless communication, and electronic warfare[1]. Traditionally, AOA parameters are usually obtained by utilizing electronic techniques, in which methods based on phase interferometers are most widely studied due to their high sensitivity and speed. However, for modern electronic technology, it is a critical challenge to meet the need of large instantaneous bandwidth. Photonic technology is well known for its large bandwidth and low loss. Up to now, a variety of photonics-based techniques have been proposed and developed for microwave measurements[2]. For AOA estimation based on microwave photonics (MWP), different optical modulators such as the Mach–Zehnder modulator (MZM)[3], dual-drive Mach–Zehnder modulator (DDMZM)[4,5], phase modulator (PM)[6], dual-parallel Mach–Zehnder modulator (DPMZM)[7], and dual-polarization dual-drive Mach-Zehnder modulator (DPol-DDMZM)[8] are generally used as photonic interferometers to map the arrival phase or time difference of the signal under test (SUT) into easily measurable parameters related to power. Although the above-mentioned methods are simple and effective, the frequency of SUT should be known in advance. However, the frequencies of noncooperative signals are unknown as well as AOA in practice. Hence, it is necessary to perform instantaneous frequency measurement (IFM) prior to the AOA estimation. To address this, some simultaneous AOA and frequency measurement methods based on MWP are presented. A concurrent photonic measuring system based on a DPMZM and an asymmetry Mach–Zehnder interferometer (AMZI) is proposed, AOA and the chirp rate of a linear frequency-modulated (LFM) signal can be measured simultaneously, which has high accuracy but is only applicable to LFM signals[9]. In Ref. [10], frequencies and AOA of multiple targets can be measured simultaneously by combining the optical time-division channelized I/Q downconversion and van Cittert–Zernike theorem. However, the channelized structure is complex.

Recently, deep learning (DL) has drawn growing attention in not only computer vision but also the signal processing of optoelectronic systems. In Ref. [11], based on data-driven supervised learning training, an adaptive deep-learning algorithm was proposed for different MWP receiving systems by changing the training data sets and retraining the same neural network. In Ref. [12], an autoencoder-residual network was designed to adaptively mitigate the nonlinearity and noise of the received broadband without the need for calculating the multifactorial nonlinear transfer functions. Additionally, the application of

DL to direction-of-arrival estimation based on array signal processing has also achieved significant success, and not only greatly improves estimation performance and generalization[13], but also can estimate the number of signal sources[14]. In summary, DL is based on a data-driven approach, which does not require setting an *a priori* observed model, but learns the model directly from the training data and adapts its own structure and parameters according to the dynamic environment and target characteristics.

In this paper, we propose a convolutional neural network with a bidirectional gated recurrent unit (BiGRU-CNN) to achieve adaptive AOA estimations without additional frequency measurements. First, the optical interferometer array with N-DDMZMs is constructed to obtain the envelope voltage vectors, which are associated with the frequency and AOA of the SUT. Then the BiGRU-CNN model is used to automatically extract features and learn the frequency information from the envelope voltage correlation matrix to establish mapping at different frequencies. Compared with the previous AOA estimation methods based on phase-to-power mapping that require extra IFM, the BiGRU-CNN exhibits strong generalization and has a simpler structure and measurement process. To the best of our knowledge, this is the first attempt to achieve MWP adaptive AOA estimation without frequency guidance based on a DL algorithm. In addition, the BiGRU-CNN model can perform IFM at a specific angle, which provides a new perspective for realizing two-dimensional parameter estimation of frequency and AOA.

2. Principle

Figure 1 shows a schematic diagram of the proposed system, which consists of four main modules: the antenna array, the optical interferometer array, the electrical processing array, and the adaptive algorithm. The antenna array consists of a reference antenna (A-0) and N measurement antennas (A-1, A-2, ..., A-N). The antenna distance between A-0 and A-i ($i = 1, 2, \ldots, N$) is d_i. Under far-field conditions, where the target source is far away from the antenna array, the microwave signal arrives at each antenna array element in the same direction, assumed to be θ. There is a time difference between the arrival of the signal at A-0 and A-i, which can be expressed as

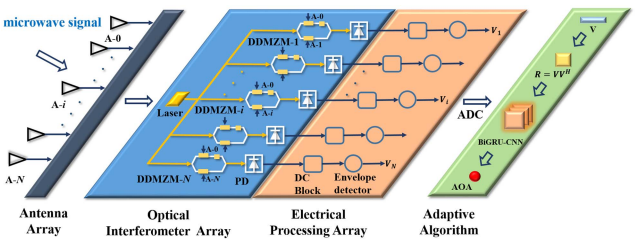

Fig. 1. Schematic diagram of the proposed adaptive microwave photonic AOA estimation system using BiGRU-CNN. *V*, envelope voltage vector; *R*, correlation matrix.

$$\tau_i = d_i \sin\theta / c, \tag{1}$$

where c is the speed of light in vacuum. The time difference τ_i causes a corresponding phase difference φ_i in the signals received by the antenna array elements,

$$\varphi_i = \tau_i \times \omega_{\mathrm{RF}} = 2\pi \frac{d_i \sin\theta}{\lambda}, \tag{2}$$

where ω_{RF} is the angular frequency of the incoming microwave signal and λ is its wavelength. The optical interferometer array includes a continuous wave laser, N DDMZMs (DDMZM-1, DDMZM-2, ..., DDMZM-N), and N PDs. DDMZM is a natural optical phase detector that can extend the operating bandwidth and achieve phase-to-power mapping, as demonstrated and widely used in Refs. [4,5]. A light wave is emitted from the laser, and then equally divided into N paths, which will be sent into each DDMZM-i channel. As is shown in Fig. 2(a), one port of DDMZM-i is driven by the signal received by antenna A-0, and the other port is from A-i. Under small signal modulation, the optical field at the output of the DDMZM-i can be expressed as

$$\begin{aligned} E_i \propto E_0 \exp(j\omega_c t) \\ \times [jJ_1(m)\exp(-j\omega_{\mathrm{RF}}t - \Phi_i) + jJ_1(m)\exp(-j\omega_{\mathrm{RF}}t) \\ + J_0(m)\exp(j\omega_{\mathrm{RF}}t) + J_0(m)\exp(j\omega_{\mathrm{RF}}t + \Phi_i) \\ + jJ_1(m)\exp(j\omega_{\mathrm{RF}}t) + jJ_1(m)\exp(j\omega_{\mathrm{RF}}t + \Phi_i)], \end{aligned} \tag{3}$$

where E_0 and ω_c are the amplitude and angular frequency of the input optical signal, respectively; J_n is the nth Bessel function of the first kind; $m = \pi V_{\mathrm{RF}}/V_\pi$ is the modulation index of the DDMZM; V_{RF} is the amplitude of the received microwave signal, and V_π is the half-wave switching voltage. Φ_i is the actual phase difference of the DDMZM's two ports,

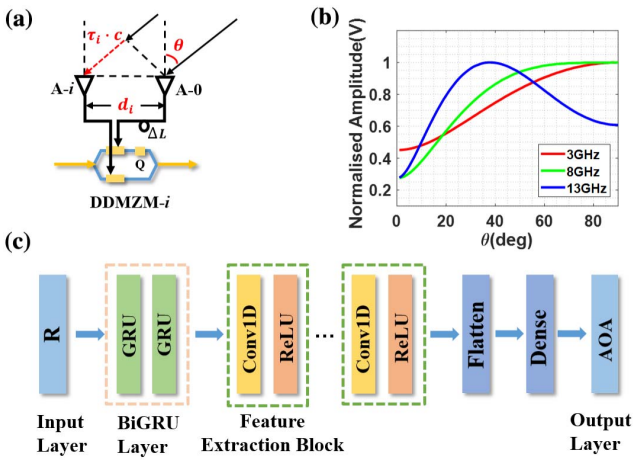

Fig. 2. (a) RF signal incident on two array elements of the DDMZM-i; (b) simulation prediction of the relationship between the output envelope voltage and AOA under different signal frequencies: d_i = 1.875 cm, ΔL = 0 cm; (c) model of the BiGRU-CNN.

$$\Phi_i = 2\pi \frac{\Delta L}{\lambda} + \varphi_i, \tag{4}$$

where ΔL is the path length mismatch of the transmission media between the antennas and the DDMZM. The electrical processing array module converts the optical signal modulated by the DDMZM to an electrical signal through a photodetector (PD). Then, the direct current (DC) associated with the optical carrier signal is removed through DC block. The detected electrical signals after the DC block can be expressed as

$$I_i \propto 2\sqrt{\frac{1-\cos\Phi_i}{2}} I = 2\left|\sin\frac{\Phi_i}{2}\right| I, \tag{5}$$

where I is the RF signal with angular frequency ω_{RF}. It can be seen that the final obtained electrical signal is a cosine function, which is related to Φ_i. To facilitate acquisition and reduce the pressure on the sampling rate, the envelope v_i of the electrical signal is obtained by an envelope detector, which has a DC voltage. Figure 2(b) shows the simulated relationship between the envelope voltage v_i and AOA under different frequencies. When d_i and ΔL are known and fixed, AOA θ and frequency f_{RF} are a pair of mutually coupled factors that together determine the envelope voltage v_i. However, a one-DDMZM channel is ambiguous at the same voltage, i.e., v_i corresponds to multiple AOA and frequencies. The number of DDMZM channels needs to be increased to obtain a set of envelope voltage vectors corresponding to the unique AOA and frequency. Therefore, by using N-DDMZM sensors, an envelope voltage vector $V = [v_i, v_2, \ldots, v_N]^T$ can be constructed that is related to AOA θ and frequency f_{RF}. We define the mapping relationship between $(f_{\mathrm{RF}}, \theta)$ and V as

$$F(f_{\mathrm{RF}}, \theta) = F(v_1, v_2, \ldots, v_N). \tag{6}$$

DL algorithms can infinitely approximate arbitrarily complex mapping relationships based on the data-driven principle. Considering that the AOA information of motion targets is continuous in reality and the correlation of samples, the AOA estimation accuracy and generalization capability will be improved using a long short-term memory (LSTM) network[15], which is suitable for processing time-sequential data. The gated recurrent unit (GRU) neural network simplifies the complex structure of the LSTM cell and has faster convergence while maintaining accuracy. The bidirectional gated recurrent unit (BiGRU) is a layer of reverse GRU added on top of unidirectional GRU. BiGRU not only improves the gradient disappearance but also increases the number of neural units, which can get more accurate prediction results[16]. Similar to array signal processing, in order to obtain the correlation between spatial signal dimensions, we map the envelope voltage vector V to a high-dimensional space to construct the correlation matrix R,

$$R = VV^H = \begin{bmatrix} v_1^2 & \cdots & v_1 v_N \\ \vdots & & \vdots \\ v_N v_1 & \cdots & v_N^2 \end{bmatrix}. \tag{7}$$

Take R as the input to the model in N time steps, and each time-step input is one row of R. To a certain extent, the data augmentation is done to V to expand N times, and the intrinsic pattern between channels can be better explored to improve the accuracy. An illustration of the BiGRU-CNN structure we employed can be found in Fig. 2(c). It mainly includes a BiGRU layer and several feature extraction blocks. The input layer inputs the normalized R into the BiGRU with the size of $N \times N$. The BiGRU layer utilizes two layers of forward and reverse GRUs to fully learn the features of the input sequence. The feature extraction block includes a one-dimensional (1D) convolutional layer used for extracting the local feature and a rectified linear unit (ReLU) as the nonlinear activation function. The flattened layer converts multidimensional feature data into 1D data. The dense layer is equivalent to the fully connected layer for nonlinear mapping, and the final output layer has only one neuron representing the predicted AOA.

3. Results and Discussion

A proof-of-concept experiment based on a three-DDMZM, shown in Fig. 3, was carried out. The light is generated by a laser diode with 1550 nm wavelength and divided into three branches through a 1×3 optical coupler (OC). All of the DDMZMs (Fujitsu FTM7937EZ200) are biased at a quadrature transmission point. The InGaAs PD, DC block, and envelope detector all have a bandwidth of 2–18 GHz. In order to provide a sufficient SNR and compensate for the link losses of the system, a low-noise amplifier (LNA) is connected after each antenna and envelope detector. Finally, the three-channel electrical signals are sampled and recorded by the Virtex-7 series field programmable gate array (FPGA) processing chip with a sampling rate of 500 MSa/s.

To ensure the authenticity of the data, data acquisition experiments were carried out in a microwave darkroom in order to exclude as much as possible the influence of external frequency bands. The receiving antenna array consists of four 2–18 GHz cavity-backed helical antennas, and the antenna separation distances were configured randomly: $d_1 = 11$ cm, $d_2 = 23$ cm, and $d_3 = 36$ cm. The SUT is generated by a signal generator (Rohde

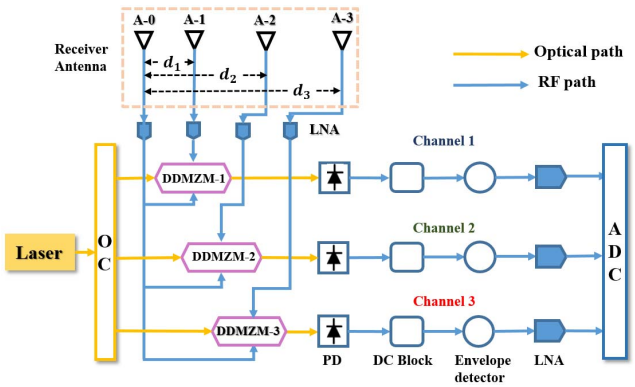

Fig. 3. Experimental setup of three-DDMZM-based AOA estimation system.

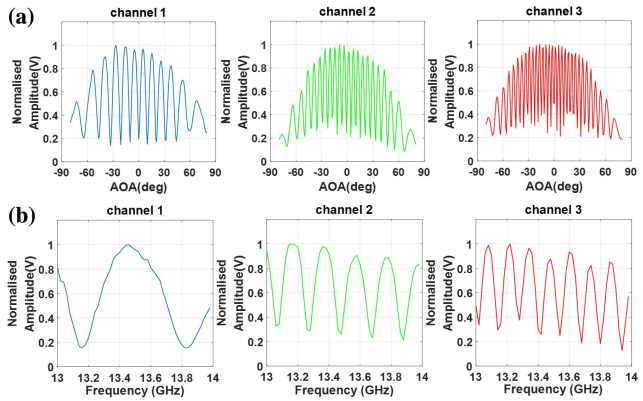

Fig. 4. (a) Normalized amplitude response for AOA at signal frequency 13 GHz; (b) normalized amplitude response for frequency at AOA 30°.

& Schwarz SMB100A) with the power of 11 dBm. The distance between the transmitting antenna and the receiving antenna array is 4 m. The envelope voltages V at different AOAs were obtained by rotating the receiving antenna array in 1° steps.

Figure 4(a) shows the normalized output envelope voltage V with respect to AOA at signal frequency 13 GHz; the frequency-amplitude response curve with an interval of 20 MHz from 13 to 14 GHz at AOA 30° is shown in Fig. 4(b). The output envelope voltage V varies periodically by changing the AOA or frequency of SUT, which means that the information of frequency and AOA can be obtained simultaneously from envelope voltage V. In order to build a clean data set for training and testing, we averaged 20 acquisitions as final samples to mitigate the random noise. A total of 483,000 samples were collected at different frequencies (3, 8, and 13 GHz) under the field of view of −80° to 80° to build the final data set. For each AOA, 64% of the data set is randomly selected for training, 16% for validation, and 20% for testing. The BiGRU-CNN model is optimized to have three feature extraction blocks. The detailed parameters of the BiGRU-CNN are shown in Table 1. After trying different hyperparameters, we find that the current one is optimal. Before being sent to the BiGRU-CNN, all the envelope voltages V are normalized and multiplied by their own transpositions to get the correlation matrix R with a size of 3×3. During the training process, the mean absolute error (MAE) is chosen as the loss function, and the Adam optimization algorithm is applied to update the network parameters with an initial learning rate of 0.01. The training epochs are set to 500, and the batch size is 200.

To avoid overfitting, the learning rate will be reduced by 10%, and training will be early stopped when the validation loss is no longer reduced after 5 epochs and 10 epochs, respectively. The training time and test time of BiGRU-CNN are about 1 h 18 min and 54 s, respectively, on a personal computer with Intel i7-6700 CPU (4-core). To demonstrate the superiority of our BiGRU-CNN model, we replace the BiGRU layer of the BiGRU-CNN model by a 1D convolutional layer with 512 filters to build a CNN model. What is more, we compare the BiGRU-CNN and CNN with and without using correlation matrix R as input. Figure 5 shows both the training loss and validation loss as the different neural network architectures concurrently decrease and converge to a small value as the epochs increase. This proves that all models are fully trained and out of overfitting. Compared with the CNN model, the combined BiGRU layer not only lowers the loss to a much lower level but also converges faster. Moreover, the use of correlation matrix R as input further enhances performance.

Table 1. Parameters of the Optimized BiGRU-CNN.

Layer	Output Shape	Units	Filter Size	Number of Filters
Input	3 × 3	/	/	/
BiGRU	3 × 512	256	/	/
Convolution-1	3 × 512	/	1 × 1	512
Convolution-2	3 × 256	/	1 × 1	256
Convolution-3	3 × 128	/	1 × 1	128
Flattened	384	/	/	/
Fully connected	128	128	/	/
Output	1	1	/	/

Figure 6 shows the experimental results and the corresponding errors over a −80° to 80° measurement range at three different frequencies. The frequency of SUT is unknown during the test. It can been seen that our BiGRU-CNN model can perform adaptive AOA estimation for three SUTs and exhibit excellent performance. The MAEs of AOA estimation at each frequency are very small, only 0.1520°, 0.1551°, and 0.1564°, respectively, which shows the system has the ability to work across octaves. In addition, the latency of single measurement is about 1.22 ms, which includes the time used for computing correlation matrix R and running the BiGRU-CNN.

To further illustrate that our model can capture and learn the frequency information of the SUT, we collected samples from 3 to 5 GHz with a step of 20 MHz at AOA of 30° as training data to perform frequency estimation. The training is also based on the BiGRU-CNN model implemented in Table 1. The final two separately trained prediction models for AOA estimation and frequency measurement are obtained, respectively. We apply

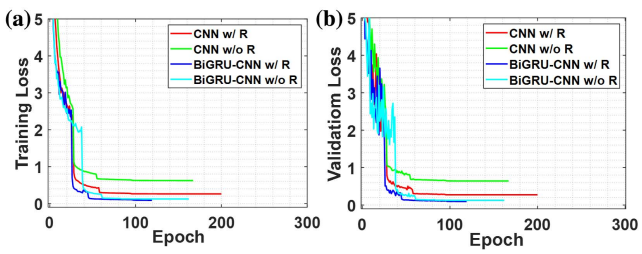

Fig. 5. (a) Training loss and (b) validation loss of different neural network architectures during training.

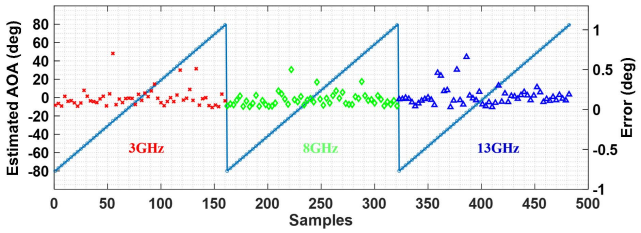

Fig. 6. Experimental results of actual AOA and estimated AOA (blue circles) and the corresponding errors at different frequencies (3, 8, and 13 GHz) over a −80° to 80° measurement range. The blue solid line represents the ideal curve for actual AOA and estimated AOA.

a 3 GHz pulsed signal (width 1 μs, period 2 μs for a 20 μs duration) that two BiGRU-CNN models have not seen before to perform frequency and AOA estimation based on two separately trained models in real time. Figure 7 shows the comparison between the actual frequency and estimated frequency, and the corresponding error is indicated by a green crossing marker. The estimated frequency within the time of pulse appears to match very well with the actual frequency. The MAE of the IFM is 10.1 MHz. On the other hand, the MAE of AOA estimation is 0.3727° during the whole pulse duration, which demonstrates that our method is capable of measuring not only continuous wave signals, but also pulsed signals.

Just like most methods based on phase-to-power mapping, the power variation of the SUT may influence the measurement results. Theoretically, the effect of SUT power can be calibrated by normalizing the output envelope signal voltage V[17]. However, for real-world applications, there exists amplitude imbalance between multiple channels because the component cannot perform ideally. To address this, the automatic gain control (AGC) module can be added after the antenna array to keep the input signal power at a stable value[18], and eventually the DL algorithm can learn these inherent errors based on a data-driven mechanism. On the other hand, although DL has shown great results in improving the performance of microwave photonic systems, it requires a large amount of experimental data, which is extremely time- and resource-consuming. In the future, to achieve AOA adaptive estimation in practical applications or even simultaneous measurement of AOA and frequency, it is not only necessary to collect data at more frequencies, but also to increase the number of DDMZM channels to solve the ambiguity problem. The number of data required is even huger. We can reduce training cost and alleviate the reliance on large numbers of data through transfer learning[19,20] or data augmentation via a generative adversarial network[21].

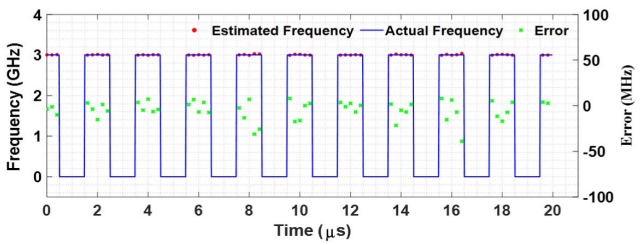

Fig. 7. Real-time IFM with 3 GHz pulse signal (width 1 μs, period 2 μs) at AOA of 30°; the frequency of 0 GHz means no signal is incident.

4. Conclusions

In conclusion, an adaptive AOA estimation algorithm using BiGRU-CNN based on an N-DDMZM array system is proposed. The BiGRU-CNN model can perform high accuracy AOA estimations of different frequency signals without additional IFM. A proof-of-concept experiment was conducted to verify the performance of the AOA estimation at three different frequencies, and the MAE is 0.1545°. Moreover, our method demonstrates the ability to perform real-time IFM at specific angles, which has great potential for further application to measure AOA and frequency simultaneously.

Acknowledgement

This work was supported by the National Natural Science Foundation of China (Nos. 61801498 and 62075240) and the National Key Research and Development Program of China (No. 2020YFB2205804).

References

1. P. Kulakowski and J. Vales-Alonso, "Angle-of-arrival localization based on antenna arrays for wireless sensor networks," Comput. Electr. Eng. **36**, 1181 (2010).
2. S. Pan and J. Yao, "Photonics-based broadband microwave measurement," J. Light. Technol. **35**, 3498 (2017).
3. J. Cai, X. Chang, W. Liu, T. Shang, and C. Li, "Photonic direction-of-arrival estimation based on compressive sensing," Appl. Opt. **60**, 3482 (2021).
4. H. Chen and E. H. W. Chan, "Simple approach to measure angle of arrival of a microwave signal," IEEE Photon. Technol. Lett. **31**, 1795 (2019).
5. L. Tang, Z. Tang, S. Li, S. Liu, and S. Pan, "Simultaneous measurement of microwave doppler frequency shift and angle of arrival based on a silicon integrated chip," IEEE Trans. Microw. Theory Tech. **70**, 4243 (2022).
6. P. Li, L. Yan, J. Ye, X. Feng, X. Zou, B. Luo, W. Pan, T. Zhou, and Z. Chen, "Angle-of-arrival estimation of microwave signals based on optical phase scanning," J. Light. Technol. **37**, 6048 (2019).
7. H. Zhuo, A. Wen, and Y. Wang, "Photonic angle-of-arrival measurement without direction ambiguity based on a dual–parallel Mach–Zehnder modulator," Opt. Commun. **451**, 286 (2019).
8. G. Li, D. Shi, L. Wang, M. Li, N. H. Zhu, and W. Li, "Photonic system for simultaneous and unambiguous measurement of angle-of-arrival and Doppler-frequency-shift," J. Light. Technol. **40**, 2321 (2022).
9. S. Li, H. Cao, and X. Zheng, "Concurrent photonic measurement of angle-of-arrival and chirp rate of microwave LFM signal," Chin. Opt. Lett. **18**, 123902 (2020).
10. Y. Yang, C. Ma, B. Fan, X. Wang, F. Zhang, Y. Xiang, and S. Pan, "Photonics-based simultaneous angle of arrival and frequency measurement system with multiple-target detection capability," J. Light. Technol. **39**, 7656 (2021).
11. S. Xu, R. Wang, X. Zou, and W. Zou, "Adaptive deep-learning algorithm for signal recovery of broadband microwave photonic receiving systems based on supervised training," J. Opt. Soc. Am. B **38**, 834 (2021).
12. L. Zhao, W. Gou, Z. Zhang, M. Shen, J. Zhang, X. Zheng, Y. Peng, and T. Jiang, "Deep-learning-assisted linearization for the broadband photonic scanning channelized receiver," Opt. Lett. **47**, 6021 (2022).

13. W. Zhu and M. Zhang, "A deep learning architecture for broadband DOA estimation," in *International Conference on Communication Technology* (2019), p. 244.
14. Y. Yang, F. Gao, C. Qian, and G. Liao, "Model-aided deep neural network for source number detection," IEEE Signal Process. Lett. **27**, 91 (2019).
15. G. Van Houdt, C. Mosquera, and G. Nápoles, "A review on the long short-term memory model," Artif. Intell. Rev. **53**, 5929 (2020).
16. X. Lin, Z. Quan, Z.-J. Wang, H. Huang, and X. Zeng, "A novel molecular representation with BiGRU neural networks for learning atom," Brief. Bioinformatics **21**, 2099 (2020).
17. G. H. Smith, D. Novak, and Z. Ahmed, "Overcoming chromatic-dispersion effects in fiber-wireless systems incorporating external modulators," IEEE Trans. Microw. Theory Tech. **45**, 1410 (1997).
18. N. Zhang, Z. Wen, X. Hou, and W. Wen, "Digital automatic gain control design with large dynamic range in wireless communication receivers," in *International Conference on Communication Technology* (2017), p. 1402.
19. S. Yi, S. Xu, and W. Zou, "Multi-band low-noise microwave-signal receiving system with a photonic frequency down-conversion and transfer-learning network," Opt. Lett. **46**, 5982 (2021).
20. E. Liu, Z. Yu, Z. Wan, L. Shu, K. Sun, L. Gui, and K. Xu, "Linearized wideband and multi-carrier link based on TL-ANN," Chin. Opt. Lett. **19**, 113901 (2021).
21. M. A. Jabin and M. P. Fok, "Data augmentation using a generative adversarial network for a high-precision instantaneous microwave frequency measurement system," Opt. Lett. **47**, 5276 (2022).